Active Participation of Membrane Lipids in Inhibition of Multidrug Transporter P-Glycoprotein

Karan Kapoor[†], Shashank Pant[†], Emad Tajkhorshid[*]

NIH Center for Macromolecular Modeling and Bioinformatics, Beckman Institute for Advanced Science and Technology, Department of Biochemistry, and Center for Biophysics and Quantitative Biology, University of Illinois at Urbana-Champaign, Urbana, IL 61801, USA

[†] *These authors contributed equally to this work*

E-mail: emad@illinois.edu

Abstract

P-glycoprotein (Pgp) is a major efflux pump in humans, overexpressed in a variety of cancers and associated with the development of multi-drug resistance. Allosteric modulation induced by binding of various ligands (e.g., transport substrates, inhibitors, and ATP) has been biochemically shown to directly influence the function of Pgp. However, the molecular details of such effects are not well established. In particular, the role and involvement of the surrounding lipid environment on ligand-induced modulation of the conformational dynamics of the transporter have not been investigated at any level. Here, we employ all-atom molecular dynamics (MD) simulations to study the conformational landscape of Pgp in the presence of a high-affinity, third-generation inhibitor, tariquidar, in comparison to the nucleotide-free (APO) and the ATP-bound states, in order to shed light on and to characterize how the inhibitor blocks the function of the transporter. Simulations in a multi-component lipid bilayer show a dynamic equilibrium between open and closed inward-facing (IF) conformations in the APO-state, with binding of ATP shifting the equilibrium towards conformations feasible for ATP hydrolysis and subsequent completion of the transport cycle. In the presence of the inhibitor bound to the drug-binding pocket in the transmembrane domain (TMD), the transporter samples more open IF conformations, and the nucleotide binding domains (NBDs) are observed to become highly dynamic. Interestingly, and reproduced in multiple independent simulations, the inhibitor is observed to recruit lipid molecules into the Pgp lumen through the two proposed drug-entry portals, where the lipid head groups from the lower leaflet translocate inside the TMD, while the lipids tails remain extended into the bulk lipid environment. These "wedge-lipid" molecules likely enhance the inhibitor-induced conformational changes in the TMD leading to the differential modulation of coupling pathways observed with the NBDs downstream. We suggest a novel inhibitory mechanism for tariquidar, and for related third-generation Pgp inhibitors, where lipids are seen to enhance the inhibitory role in the catalytic cycle of membrane transporters.

Introduction

ATP-binding cassette (ABC) transporters form one of the largest transporter superfamilies expressed in cellular plasma membranes[1–3] and involved in the efflux of small molecules out of the cell.[4,5] ABCB1, or P-glycoprotein (Pgp), a prominent member of this superfamily, is ubiquitously expressed in different tissues[6] where it exports a wide range of charged and neutral hydrophobic molecules.[7] This promiscuous quality of Pgp is exploited by, e.g., cancer cells that over-express the transporter in their cellular membranes, and thereby acquire resistance to chemotherapeutic reagents and other drug molecules.[8] In this context, a major drug development effort has been in the direction of inhibiting Pgp and therefore achieving more effective chemotherapeutic treatments from the currently used anticancer drugs. In order to make such efforts more effective, it is imperative to understand the workings of the transporter in its physiological context, i.e., the cellular membrane, which will more likely allow for discovery of novel inhibition mechanisms and drug development.

Structurally, Pgp shows a pseudo two-fold symmetry, folding into a single-chain heterodimeric structure containing two transmembrane domains (TMDs), each consisting of a six-helical transmembrane leaflet associated with a nucleotide-binding domain (NBD).[9–12] The two drug-entry portals proposed to exist within the transmembrane region of the transporter are located on either side of the TMDs and allow access of molecules from within the membrane to the large, central, semi-hydrophobic lumen of Pgp.

Substrate translocation in ABC transporters like Pgp involves complex structural changes from an inward-facing (IF) to an outward-facing (OF) state, alternatively exposing the substrate binding site/region to inside and outside of the cell, a model coined as the "alternate access".[13,14] In Pgp, this mechanism facilitates the export of substrate molecules out of the cell.[15–22] The conformational coupling between the NBDs and the TMDs is key to the ATP-driven transport in Pgp and other ABC transporters. Without getting into specifics, in this transport scheme, ATP-binding to the two NBDs promotes their dimerization, with the resulting conformational changes directly coupled to the TMDs and their subsequent

formation of the OF state.[16,17] Hydrolysis of ATP, on the other hand, releases the dimerized NBDs, allowing the transporter to reset to the IF state.[23,24] Through these general couplings, ATP binding and hydrolysis in the NBDs mechanically control the interconversion between the IF and OF, and therefore, the accessibility of the substrate between the two sides of the membrane.

As a multi-domain protein, Pgp exhibits a complex behavior, with the binding of ATP, substrates and inhibitors directly modulating the conformational state and characteristics of the transporter.[25] Experimental Pgp structures, often resolved in a non-membrane environment, have often found the transporter in open-IF(-like) states, characterized by large separations between the two TMD leaflets on the cytoplasmic side, and between the two NBDs.[9–12] Other experimental studies conducted in a similar non-native environment (e.g., micelles), as well as using different protein constructs, have presented similar results regarding the mechanistically relevant conformational states of the transporter.[26–29] On the other hand, biochemical studies performed in more realistic and physiological environments (e.g., nanodiscs or other lipid bilayers), have presented an alternate view of the transporter's mode of action, where the APO (nucleotide-free) and ATP-bound transporter states are present in a thermodynamic equilibrium capable of sampling similar conformations,[30–32] highlighting the importance of the lipid bilayer in regulating Pgp's conformational dynamics.

A number of studies have also aimed at developing novel molecules for targeting this biomedically important transporter.[33] Out of these, third-generation inhibitors, displaying high binding specificity for Pgp, provide the most promising candidates. Tariquidar (TAR), one such high-affinity, third-generation inhibitor that binds to the central cavity of Pgp, has been suggested to function by destabilizing NBD conformations necessary for ATP hydrolysis.[29] Recent structural studies have provided additional static information on the location and binding mode of this class of inhibitors,[34] but the mechanism of action of these molecules remains unclear.

Here, we present a molecular dynamics (MD) study providing an atomic-level description

of the conformational dynamics of Pgp in the APO, ATP-bound, and TAR-bound states, and propose a model connecting these changes to the possible transport and inhibition mechanisms of Pgp. Our MD simulations capture a dynamic equilibrium between the open and closed IF conformations in APO Pgp, with ATP binding observed to promote NBD dimerization and closing of the cytoplasmic gate. Compared to the APO and ATP-bound states, TAR-bound Pgp shows highly dynamic NBDs and TMD portal regions, sampling more widely open IF conformations. We also observe a substantially enhanced inhibitor-mediated recruitment of the membrane lipids into the central lumen of the transporter, which together with the inhibitor binding itself result in a differential allosteric coupling between TMD and NBDs, highlighting an important role of lipids in modulating the conformational landscape of Pgp and its inhibition. The study provides a new direction for future drug-discovery endeavours, targeting challenging proteins like Pgp, through the development of molecules that can successfully modulate the lipid environment, and thus, the active conformational ensemble of the protein.

Methods

In order to characterize the conformational dynamics of Pgp in the presence and absence of the third-generation inhibitor TAR, we modeled and performed atomistic simulations of 3 different systems, namely, APO (nucleotide-free), ATP/Mg^{2+}-bound (also termed the ATP system), and TAR-bound. We discuss the system construction and the MD methodology in the following sections.

System Preparation

A recent crystal structure of Pgp (PDB: 4M1M)[12] in the IF state was used as the starting point for constructing APO, ATP/Mg^{2+} and TAR-bound structures. For the generation of the APO system, only chain B was retained from the PDB structure, containing residues

34-626 and 696-1,271. The missing region (residues 627-695) corresponds to a flexible linker region connecting NBD1 to the TMD2, not resolved in any available structure of Pgp and was not included in the simulations. For the generation of the ATP/Mg^{2+}-bound system, ATP molecules were docked into their respective binding sites in the two NBDs using a rigorous protocol described by Wen et al,[35] which reproduces the nucleotide binding characteristics observed in the high-resolution crystal structure of another ABC transporter, HlyB.[36] For the generation of the TAR-bound system, we used a variant of ensemble docking, termed as extended-ensemble docking, that first captures the conformational ensemble of the protein (Pgp bound to ATP/Mg^{2+} in this case) using steered MD simulations along specific collective variables,[37] and then utilizes these conformations for docking purposes. Using the protocol described by Kapoor et al. (unpublished data), the docked structure showing the strongest predicted binding affinity (highest docking score) was selected as the starting TAR-bound system. This TAR-bound structure shows a Cα root mean squared deviation (RMSD), of 3.8 Å with respect to the starting APO structure. Of importance to our comparative study here, the initial TAR-bound structure is also in an IF state, similar to the APO and ATP initial systems simulated.

Membrane Embedding

To study the conformational dynamics of Pgp in APO, ATP/Mg^{2+}, and inhibitor-bound states, we carried out multiple all-atom MD simulations for the three systems in explicit anionic lipid bilayers, mimicking conditions used in recent FRET and DEER studies on Pgp.[29,31] Five independent lipid bilayers containing anionic phospholipids (PC (40%), PE (43%), PG (14%), and CL (3%)) were constructed using the membrane-builder module of CHARMM-GUI,[38] and each state of the protein was inserted into these membranes independently. Subsequently, Pgp was inserted into the membrane and the overlapping lipids removed from the bilayer (Fig. 1).

It is to be noted that in order to remove any bias generated due to the initial distribution

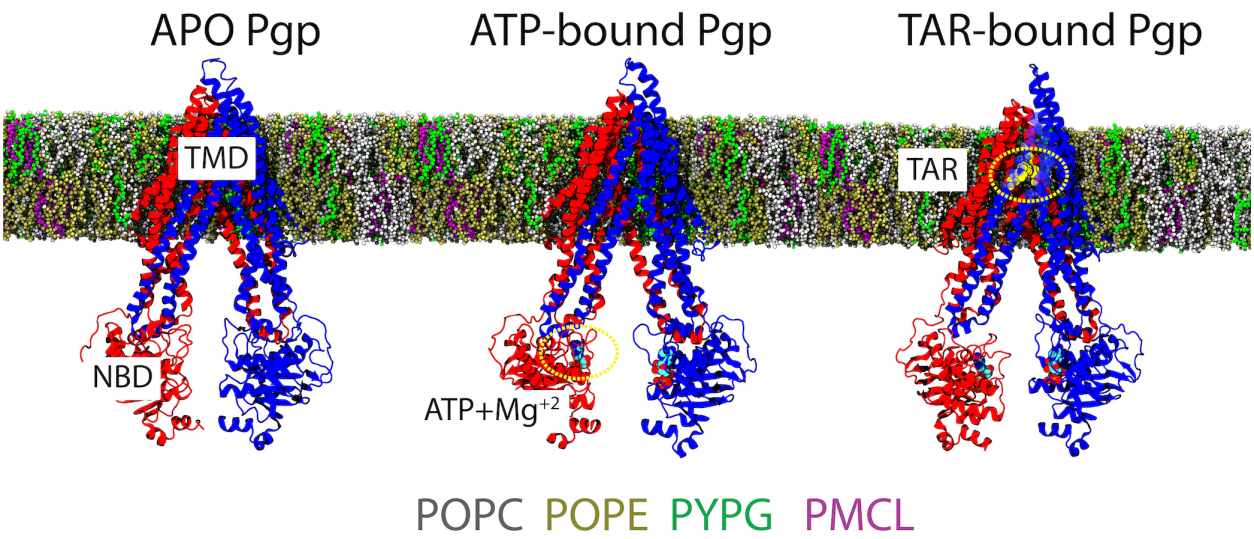

Figure 1: **Simulation systems:** APO, ATP/Mg^{2+}-bound, and TAR-bound IF conformations of Pgp used in the simulations, with the two TMD leaflets, each connected to a NBD, colored in red and blue (see Methods for details on system construction). All the bound states were inserted in lipid bilayers containing: phosphatidylcholine (PC=40%), phosphoethanolamine (PE=43%), phosphoglycerol (PG=14%), and cardiolipin (CL=3%) lipids, shwon in different colors.

of lipids, all the lipids molecules occupying the central cavity of Pgp and/or penetrating the two TMD portals were specifically removed. Thus, two strategies were employed for sampling the conformational space of the studied systems: (A) randomizing the initial distribution of lipids around Pgp, and (B) randomizing the initial velocities of the atoms (Table 1).

In addition to the above-described three bound states, we also performed simulations of the starting TAR-bound Pgp conformation in the absence of the bound inhibitor. This was done so as to check the stability of the starting TAR-bound Pgp conformation, as well as a point of comparison to the starting conformations of the APO and ATP-bound systems. We term this structure as the "TAR-less" system or the "control" simulation.

MD simulations

All the simulations were performed using NAMD2.[39,40] CHARMM36m protein and lipid force field[41,42] and TIP3P water[43] were used. The inhibitor molecule (TAR) was parametrized using the `force field ToolKit (ffTK)` plugin[44] implemented in VMD.[45] Briefly, all the

ab-initio calculations (geometry optimization, and calculation of bonded, electrostatic, and torsional terms) were performed using second order Moller-Plesset (MP2) theory[46] and the 6-31G(d) basis set in Gaussian09.[47] After geometry optimization, partial charges were assigned using quantum mechanical calculations. The bonds and angular terms were calculated directly from the Hessian, and the dihedral parameters were fit to the QM potential energy landscape.

The protonation states of the ionizable residues of Pgp were calculated using the `PropKa` server.[48] The C-terminal carboxylate capping group, N-terminal ammonium capping group, and all the hydrogen atoms were added to the structures using the `PSFGEN` plugin of VMD.[45] All systems were solvated and neutralized with 0.15 M NaCl. The final systems contained ∼250,000 atoms with approximate dimensions of $135\times135\times190\,\text{Å}^3$.

All the simulations were performed at 310 K maintained using Langevin thermostat with a damping coefficient of $\gamma = 1\,\text{ps}^{-1}$. Constant pressure was maintained at 1 bar using the Nose-Hoover Langevin piston method.[49] The particle mesh Ewald (PME) method[50] was used in calculating the long-range electrostatic forces. A 12-Å cutoff distance and a 10-Å switching distance were used in calculating the non-bonded forces. An integration timestep of 2 fs was used in all simulation runs. The system was initially minimized and equilibrated for 10 ns with the Cα atoms restrained to their initial positions with a force-constant $k = 1\text{kcal/mol/Å}^2$. All restraints were then released in the following production run. With the aim of better sampling lipid-protein interactions, we extended MD simulations for 3 replicates of each system (APO, ATP-bound and TAR-bound Pgp) to 500 ns. Additionally, a 200-ns control simulation of the TAR-less system was also carried out (Table 1).

Analysis

The conformational dynamics of Pgp were characterized in terms of the large-scale motions of the different domains of the transporter, as well as secondary structure changes in the different simulated systems. As the surrounding lipid environment can play a significant role

Table 1: Details of the systems and the simulations performed.

Protein (Pgp)	**No. of independent membrane patches**	**No. of replicas per patch**	**Time/replica (ns)**
APO	5	2	200, 500*
ATP-bound	5	2	200, 500*
TAR-bound	5	2	200, 500*
Control**	1	1	200

* Simulation time was extended to 500 ns for three replicas each of APO/ATP/TAR-bound systems.
** MD simulations performed on TAR-bound Pgp conformation after removing the bound TAR molecule.

in modulating the conformational ensemble of membrane proteins, we characterized the lipid density and penetration inside the protein in the different systems, as well. Additionally, we also characterized the potential conformational coupling between the TMD and NBDs of Pgp, as the structural changes observed in the different systems may differentially affect the communication between these domains. Analysis on the conformational changes in the protein was carried out on all the simulation runs, whereas calculation of lipid properties around the protein was done on the three replicates of each systems that were extended to 500 ns. All analyses wer performed using our in-house scripts and/or VMD plugins.

Global conformational dynamics. ABC transporters, and in particular ABC exporters, are highly dynamic systems undergoing complex structural changes in both their TMD and NBDs. The global conformational dynamics of Pgp in all the simulated systems were monitored based on a set of orientational collective variables that have been previously used to successfully describe the alternate-access transport model[13] in homologous ABC transporters.[37,51] Briefly, α is defined by the relative orientation of the two TMD leaflets and describes the cytoplasmic opening of the TMDs. The angle γ is defined by the relative orientation of the two NBDs and describes their twist angle as they approach each other (Fig. S1). Additionally, distances were calculated between different domains of the transporter: (a) between the C-α atoms of residues S92 and R745 located at the extracellular side

of Pgp (d_{ext}), (b) between the C-α atoms of residues K145 and M787 located in opposite leaflets (d_{TMD}), and (c) between the center of mass of the two NBDs describing their degree of dimerization (d_{NBD}) (Fig. S1). These orientational and distance-based metrics together capture major conformational changes in the TMDs and the NBDs of Pgp.

Local conformational dynamics. The recently reported structures of Pgp display specific differences in their secondary structure, especially in their TMD.[34,52] In addition to the global conformational changes, we thus quantified the local changes (defined for the immediate region surrounding the central cavity where the inhibitor binds) in Pgp in the different simulated systems. For this, we calculated the root mean square fluctuations (RMSF) of all the residues and the secondary structure content of the portal helices (TM4, TM6, TM10, and TM12). Both the calculations were performed in VMD.

Lipid density around protein. The surrounding lipid environment can play a significant role in modulating the structural dynamics of the membrane proteins. The role of the surrounding lipidic environment was thus evaluated by calculating the lipid distribution around Pgp in all the simulated systems. The lipid density profiles were calculated by selecting the lipid head group heavy atoms lying within 20 Å, from the surface of Pgp (defined by all protein heavy atoms). All the analysis was performed for the three 500-ns-long MD replicates for each bound state.

Lipid access events through portals. Differences observed in lipid density around the protein, as discussed later, also pointed to possible differences in lipid access inside the protein. We therefore calculated the lipid-access events inside the central cavity of Pgp for all the three studied systems. The central binding region of Pgp is formed by residues from the TM1, TM2, TM3, TM5, TM7, TM8, TM9, TM11, and TM12 helices present in the membrane region. A lipid access event was counted if the phosphate head group of a lipid molecule accessed the cylindrical region defining this cavity at any point during the

simulation. To evaluate the behavior of lipids that access the Pgp central binding region, the z coordinate profiles for the center-of-mass of all the lipid head groups with respect to the membrane center (lying at $z = 0$) were monitored over the course of the simulation.

Lipid interacting residues in TMD portals. The lipid-protein interaction analysis was performed to identify the drug-entry portal residues forming the hotspots for lipid interactions on the surface of Pgp. The entry portals are delimited by the helices TM4 and TM6 (Portal 1) and by TM10 and TM12 (Portal 2). The hotspots for lipid interactions in these entry portals were identified whenever the phosphate head group of a lipid molecule came within 3 Å of the portal residues. The heavy atoms of the following residues were considered at the portals: K230-H241 of TM4, S345-G356 of TM6, L875-K883 of TM10, and Y994-S1002 of TM12. These calculations were done for the entire trajectory, giving the number of times a residue forms contact with the lipid molecules.

Network analysis for allosteric coupling. The transport cycle of ABC transporters involves large conformational changes in both TMD and NBDs, which relies on complex communication pathways between the two domains. Coupling between TMDs and NBDs can somewhat be studied in terms of the pathway of residues that efficiently transmit force between the two domains. To investigate the inter-domain communication, dynamic network analysis was performed on different Pgp systems using the `Network-View` plugin[53] of VMD. In a network, all C-α atoms are defined as nodes connected by edges if they are within 4.5 Å of each other for at least 75% of the MD trajectory. At first, Pearson correlation was used to define the communities in the entire network corresponding to the set of residues that move in concert with each other. Furthermore, the coupling between the TMDs and NBDs was defined as the path connecting a source and a sink. The source was defined as the residue S988, located on the portal helix TM10 that shows major conformational variability between the three simulated bound states. The sink was defined by Q1114 of the conserved Q-loop region of the NBD, making contacts with the coupling helices in the TMDs and important

for coupling conformational changes between the NBDs and the TMDs.[54] It is to be noted that all the residues falling in the force propagation pathways need not be considered vital for allostery. The network analysis was performed on the 500-ns MD trajectories for all the three bound states.

Validation of inhibitor docked pose. In order to further validate the stability of the starting binding mode of TAR in the Pgp central cavity, as captured from our extended ensemble docking studies, we monitored two complementary properties: (1) calculating the RMSD of TAR with respect to Pgp from the 500-ns simulations, and (2) calculating the contacts between the heavy atoms of TAR and its binding pocket residues. A distance cut-off of 3.5 Å was used to calculate these contacts. Furthermore, we compared these contacts with a recent cryoEM structure of Pgp in complex with another high-affinity, third generation inhibitor, zosuquidar.[55]

Results

Multiple all-atom MD simulations of Pgp in APO, ATP- and inhibitor-bound states allowed us to characterize major structural and dynamical differences between these states, also highlighting the influential and differential role played by the lipids in the dynamical properties of the three systems. The results presented here are primarily divided into three sections describing: (1) global and local conformational dynamics of Pgp in different bound states, (2) lipid-mediated structural modulation of Pgp, and, (3) allosteric coupling between the TMDs and NBDs.

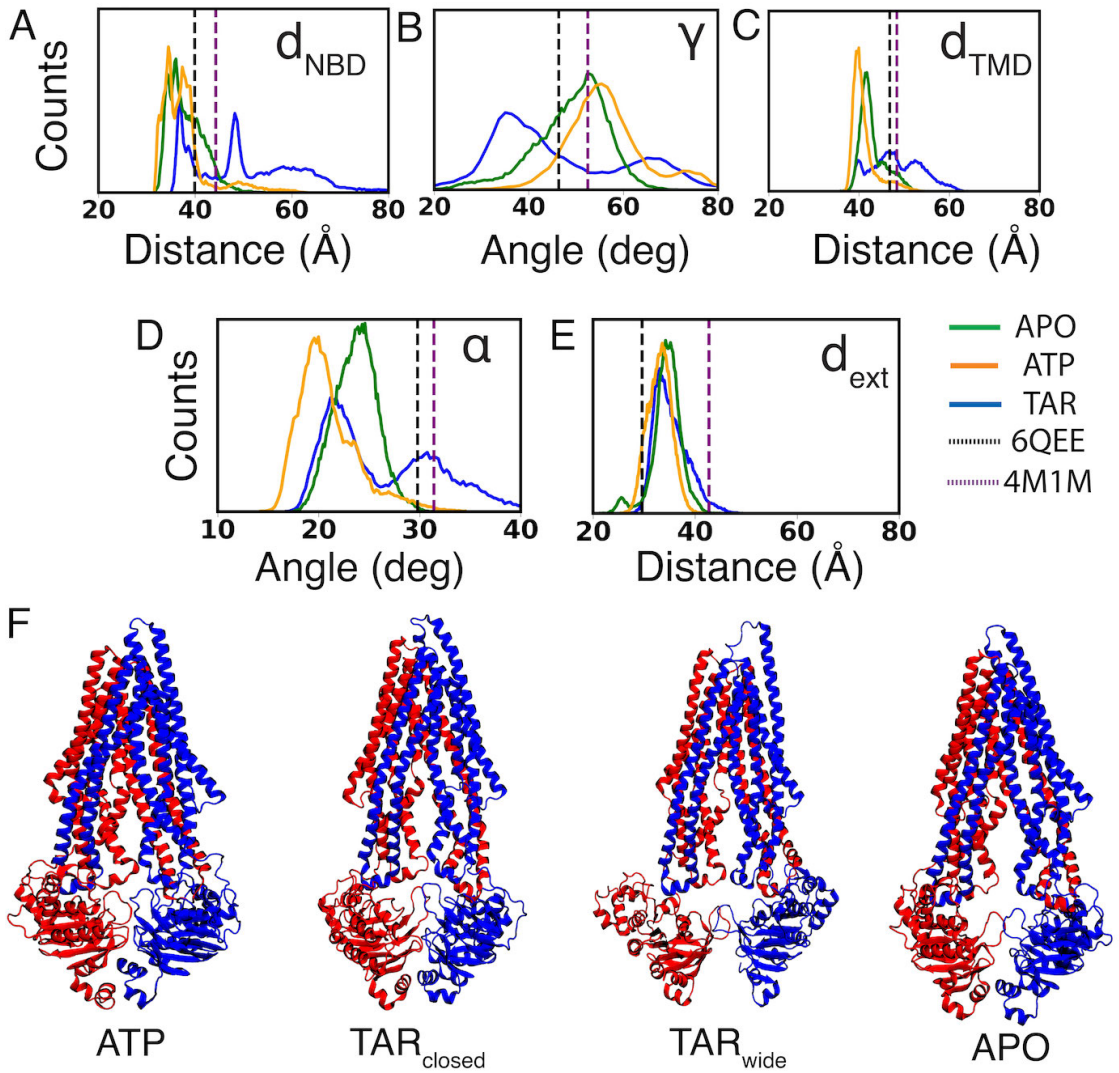

Figure 2: **Conformational variability in Pgp:** Conformational dynamics in all the simulated systems were evaluated by analyzing: (A) d_{NBD}: the center of mass distance between the two NBDs, (B) γ: relative orientation (twist) of the two NBDs, (C) d_{TMD}: the center of mass distance between the residues Q145 and N747, (D) α: relative orientation of the TMD helices describing the cytoplasmic opening, and (E) d_{ext}: the center of mass distance between the residues S92 and R745. Structural description of these parameters is provided in Figure SS1. The histogram plots of our entire dataset show the presence of more widely open IF conformations of Pgp in the TAR-bound state (shown in blue), compared to APO (green) and ATP (green) systems. Dotted vertical lines in each panel mark the values in the recent structures for an inhibitor (zosuquidar)-bound Pgp (PDB:6QEE)[34] (black) and for APO Pgp (PDB:4M1M)[12] (purple). Time series of the distances shown in the histograms are provided in Fig. S2. (F) Representative snapshots for ATP, TAR_{closed}, TAR_{wide}, and APO are shown.

Conformational dynamics of different Pgp bound states

Global conformational dynamics

The global conformational dynamics of Pgp in the APO, ATP-bound and inhibitor-bound systems were characterized in terms of the orientation and the inter-domain distances of different domains. The transmembrane conformational dynamics in Pgp were described by α, defining the degree of closing on the cytoplasmic side, and inter-residue distances calculated at the base as well as apex regions of the TMDs (d_{TMD} and d_{ext}, respectively). The degree of NBD dimerization was described in terms of the twisting angle between the NBDs, γ, and the respective separation between their centers of masses (d_{NBD}). During the simulations, the ATP systems show significant closing and more frequent dimerized-like states of the NBDs compared to the starting crystal structure (Fig. 2A,B,F and Fig. S2). On the other hand, the inhibitor-bound (TAR) systems show highly dynamic NBDs, both in terms of the distance and the twist angle between them, sampling two distinct conformations defined based on their NBD separation: if d_{NBD} is greater than 42 Å we call that conformation as TAR_{wide}, otherwise as TAR_{closed} (Fig. 2). In the APO systems, we observe a dynamic equilibrium between the open- and closed-IF conformations, and relatively higher populations for the open NBD conformations compared to the ATP systems.

Similar to NBD distances, a significant degree of TMD closing (d_{TMD}) is observed for the ATP systems, whereas the APO systems show relatively more open TMD conformations (Fig. 2C and Fig. S2). The TAR systems sample a wider range of d_{TMD}, lying on either side of the starting crystal structure. In terms of the cytoplasmic closing (α), the ATP systems show smaller TMD angles as compared to APO (Fig. 2D and Fig. S2). The TAR systems show TMD cytoplasmic angles similar to the APO systems, as well as a larger population similar to the starting crystal structure and the recent cryoEM structure of Pgp bound to zosuquidar.[55] We note that in all the simulated systems, TAR remains stably bound inside the central cavity of Pgp (Fig. S3). Additionally, comparison of the TAR-bound simulations

with the zosuquidar-bound Pgp structure shows a large similarity between the interactions of the two molecules with the protein (Fig. S3). Pgp may thus display a shared (conserved) binding site for these two molecules, and possibly other third-generation inhibitors in general.

Due to the limited timescales of our simulations, Pgp does not sample conformations in the occluded or OF states, thus no significant changes are noticeable in the extracellular opening (d_{ext}) (Fig. 2E and Fig. S2). The control simulation of the TAR-bound conformation (after removing the bound inhibitor) displays dynamical behavior similar to the ATP-bound Pgp, supporting the structural similarity of the two protein conformations used to initiate these two simulations (Fig. S4).

Local conformational dynamics

The differences in the local fluctuations in the three bound states were characterized by calculating the RMSF of all the protein residues. In inhibitor-bound systems, NBD residues were observed to be more dynamic when compared to the APO and ATP systems (Fig. S5A, B, C and D).

Additionally, residues in the portal helices, TM4 and TM6 comprising Portal 1, and TM10 and TM12 comprising Portal 2, lying on the opposite sides of the TMD, are significantly more dynamic in the TAR systems compared to the ATP and APO systems. In order to further evaluate the structural dynamics of the portal helices, which show large local fluctuations, their secondary structure content was calculated over the course of the simulations. TM10, initially present as a structured helix, was found to be partially unfolded in the inhibitor-bound simulations (Fig. 3A, B). A similar, broken TM10 helix is also captured in the recent cryoEM structure of zosuquidar-bound Pgp.[34,55] This helix maintains its helicity in ATP simulations, whereas the APO system shows a helicity between the ATP- and inhibitor-bound systems (Fig. 3A, C and D). Except for TM12, which is partially unfolded in the starting crystal structure, no unfolding was observed in other portal helices (TM4 and TM6) (Fig. S6).

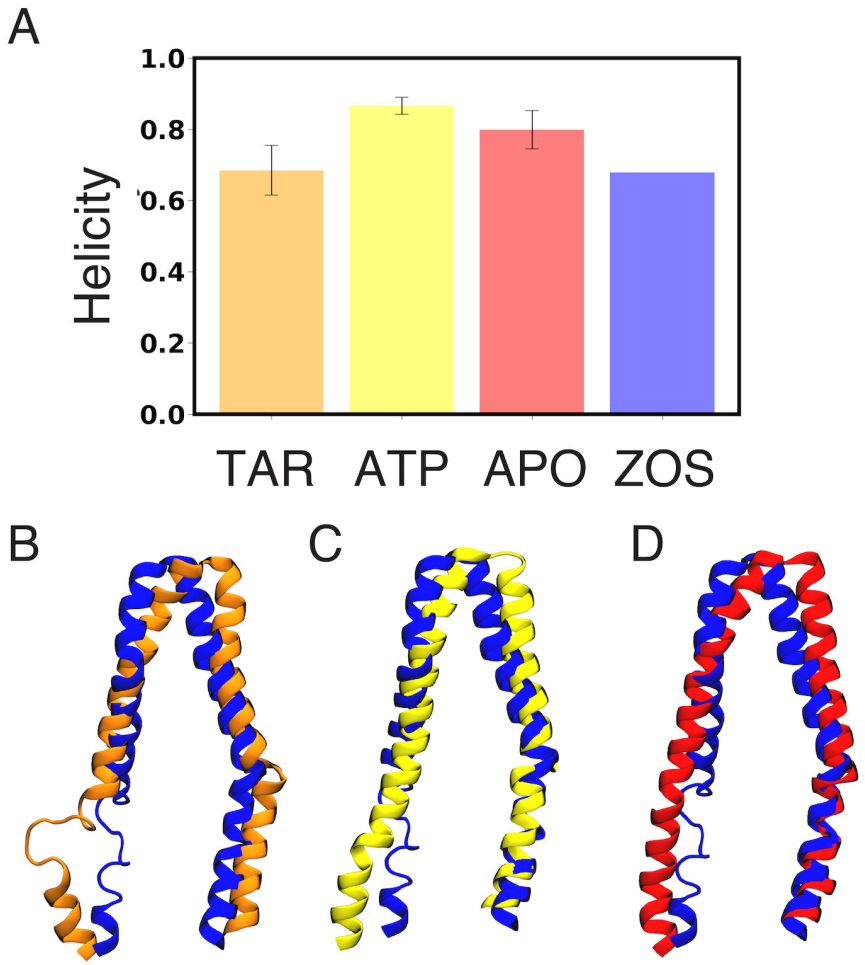

Figure 3: **Differences in secondary structure:** (A) Comparison of the degree of helicity in portal helix TM10 (resid: 876-889) in APO, ATP, and TAR Pgp with the zosuquidar-bound (ZOS) Pgp cryoEM structure.[55] The analysis was performed combining all three 500-ns simulations for each state. The structure of TM10 in a representative trajectory snapshot from: (B) TAR-bound (orange), (C) ATP (yellow), and, (D) APO Pgp (red) aligned with zosuquidar-bound Pgp[55] (blue). Helicity of other portal helices (TM4, TM6, and TM12) is shown in Fig. S6.

Lipid-mediated structural modulation of Pgp

The role of membrane lipids in modulating the structural properties of Pgp was further evaluated by calculating the lipid distribution and packing around the protein as well as lipid penetration/translocation inside the central cavity of Pgp.

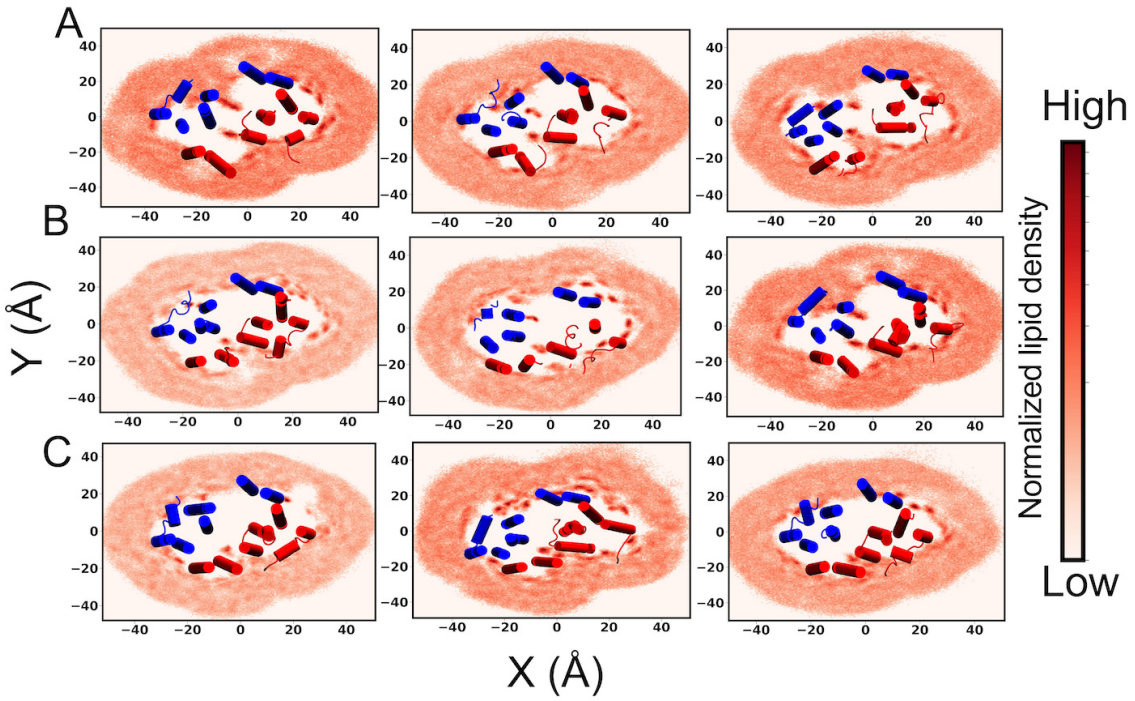

Figure 4: **Lipid packing around Pgp:** The lower-leaflet (cytoplasmic) lipid density profile for (A) TAR-bound, (B) APO, and (C) ATP-bound Pgp was calculated for all the three 500-ns MD simulations. The system is aligned along the Z-axis and viewed from the extracellular side of the protein, with the xy indicating the plane of the membrane. The lipid density was calculated by plotting the 2D histogram of the position of the phosphorous atoms (throughout the trajectories) within 20 Å of the protein surface. Each plot histogram was normalized. The lipid molecules access the central cavity through the entry portals.TAR-bound and APO Pgp showed enhanced lipid density inside the central cavity of Pgp, while a low density was observed in the case of ATP-bound systems. A cross-section of Pgp (taken at the end of 500-ns long simulation) is shown in cartoon representation.

Lipid packing around Pgp

To probe the role of the surrounding lipidic environment in modulating the global and local conformational dynamics of Pgp, we first calculated the distribution of lipids around the transporter from our simulations. In the inhibitor-bound systems, a large density of lipids was observed in the central cavity, lipids that originate from the cytoplasmic leaflet through the two TMD entry portals (Fig. 4A). The APO systems also show lipids inside the central cavity, though to a smaller degree compared to the TAR systems. In the ATP systems, on the other hand, lipid density is only observed inside the Portal 1 (Fig. 4B and C). All lipids accessing the central cavity in the simulated systems originate from the cytoplasmic leaflet of

the membrane, in agreement with the results of a previous coarse-grained simulation study,[56] clearly related to the more open configuration of Pgp in the cytoplasmic half.

Lipid access events through TMD portals

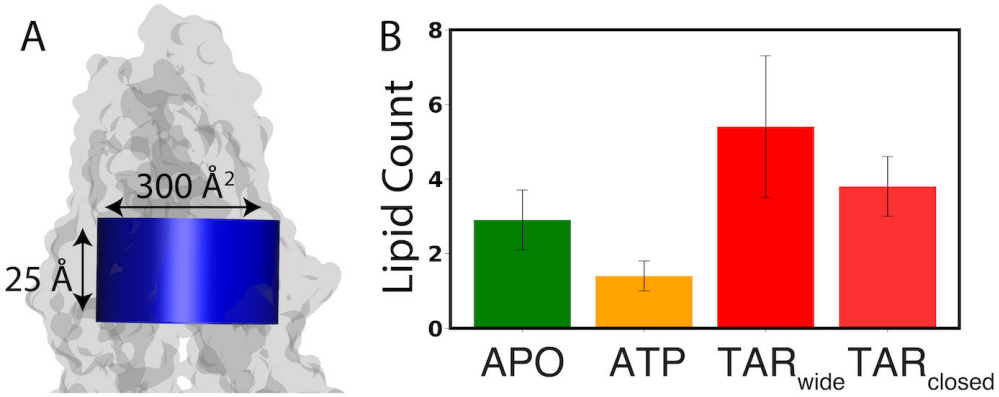

Figure 5: **Lipid access into the lumen of Pgp:** (A) A lipid access event was counted if any lipid molecule accesses the central cavity of Pgp, defined by a cylinder (shown in blue) with a cross-sectional area of 300 Å^2 and a height of 25 Å (see Methods for the criteria used to define the boundaries of the central cavity). Pgp is shown in a translucent surface representation. (B) Count of lipids accessing the central cavity of Pgp through the entry portals in APO (green), ATP (orange), TAR-bound (red) simulations, calculated by counting the number of phospholipid head groups accessing the central cavity over the course of the 500-ns simulations. Two TAR-bound conformations (TAR$_{wide}$ and TAR$_{closed}$) are defined based on the d$_{NBD}$ separation, as discussed above. In comparison to the APO and ATP-bound Pgp, more lipid access events are observed in the TAR-bound systems, especially for the TAR$_{wide}$ conformations.

The number of lipid access events in the simulated systems was calculated by monitoring the positions of lipid head groups assessing the central cavity of Pgp, defined as a cylindrical region (Fig. 5A), over the course of the simulations. As expected, the maximum number of access events is observed for the inhibitor-bound systems, especially for TAR$_{wide}$ conformations, and the minimum number of events for the ATP systems (Fig. 5B). Consistent with the higher lipid densities observed inside the central cavity for the APO systems compared to the ATP systems, lipid access events were also found to be relatively higher in the former case.

The key Pgp residues involved in lipid recruitment through Portal 1 and 2 were deter-

mined by monitoring the portal residues which make contacts with the lipid head groups over the course of the simulation (Fig. S7A). Both entry portals are observed to be rich in basic residues that directly interact with the negatively charged phosphate groups of lipids: R355, K238, and K230 at Portal 1, and K881 and K996 at Portal 2 (Fig. S7B and C).

Translation of lipid molecules in TAR-bound Pgp

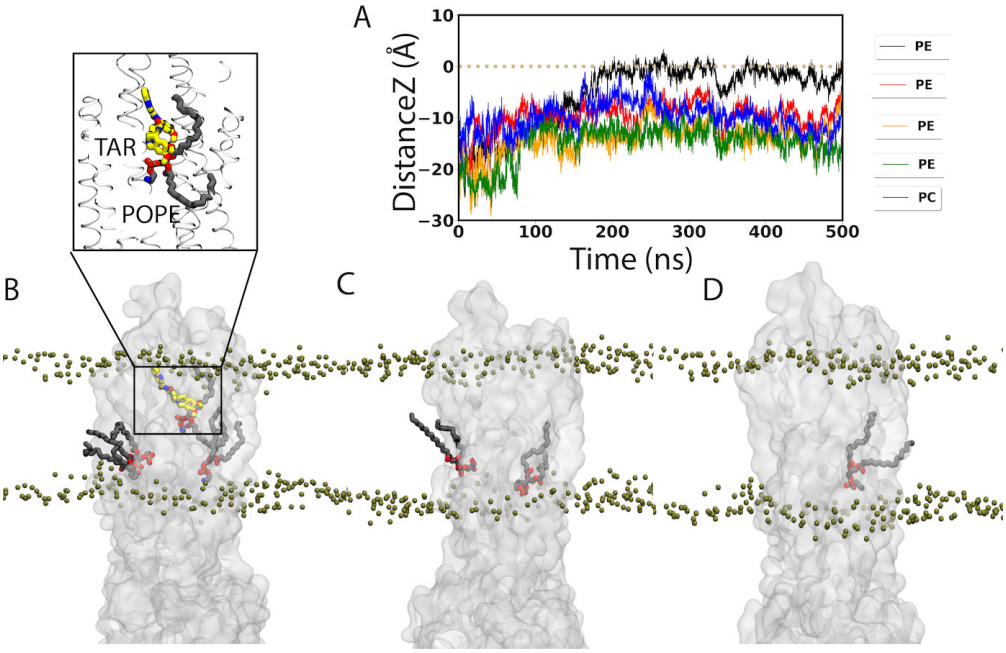

Figure 6: **Trans-leaflet lipid diffusion inside Pgp:** (A) Lipid flipping events in the central cavity of Pgp were evaluated by calculating the z center of mass movement of the lipid head groups in the three 500-ns simulations. The position of the lipid bilayer midplane is marked with a pink dashed line. Lipid flipping of PC and PE lipids was only observed in the TAR-bound Pgp, where lipid molecules from the lower (cytoplasmic) leaflet translated towards the center of the lipid bilayer. (B-D) Lipids (van der Waals representation) present in the central cavity of (B) TAR-bound, (C) APO and (D) ATP Pgp (translucent surface representation) from representative snapshots of the simulations. Phosphate atoms from the lipid head groups are shown in grey bead representation to delineate the membrane boundary. Inset in (B) shows the closeup view of the interactions between the bound TAR and the flipped lipid (PE) molecule showing the largest translation (black trace in (A)) towards the membrane center.

To evaluate the behavior of lipids that access the Pgp binding cavity, the membrane positioning (z coordinate) of the lipid head groups accessing the central cavity was monitored

over the course of the simulation. Interestingly, in TAR_{wide} conformations, large tranbsmembrane translations of lipid, which we term lipid flipping events were observed. During these events, lipid head-groups from the lower leaflet translated along the membrane normal and flipped towards the upper leaflet (see an example of such events in Supp. Video 1), forming direct interactions with the bound inhibitor in the central cavity (Fig. 6A and B). The lipids translating beyond the membrane center show formation of close and stable interactions with TAR for rest of the simulation time. The lipid tails of these 'wedge-lipids' remain protruding into the bulk membrane through the entry portals (Fig. 6B). No flipping events were observed in either APO or ATP systems (Fig. 6C and D) as well as in the control simulation after removing the bound inhibitor. It is to be noted that compared to other lipids, a higher percentage of PE lipids are present in our simulated membranes, thus increasing the portal access as well as translation probability for this lipid type in our simulations.

Conformational coupling between TMDs and NBDs

Dynamic network analysis was employed to understand the allosteric coupling between the NBDs and TMDs in the different simulated systems. The force propagation pathway was calculated between TM10 helix in the TMD, which shows major conformational differences between the three systems (as described above), and the conserved Q-loop in NBD, which is important for coupling conformational changes between NBDs and TMDs and subsequent conformational transition between the IF and OF states of Pgp.[54,57]

The APO and ATP systems predominantly show short and direct force propagation pathways connecting the TM10 with the Q-loop (Fig. 7A and B). In the case of the ATP systems, the pathway connects the TMD with the NBD directly through the coupling helices located at the interface of TMD and NBD, whereas in the APO systems, the pathway connects the two domains without directly passing through the coupling helices.

In the case of the inhibitor-bound systems, on the other hand, extended pathways are observed passing through additional portions of the NBD (Fig. 7C). In some cases, the

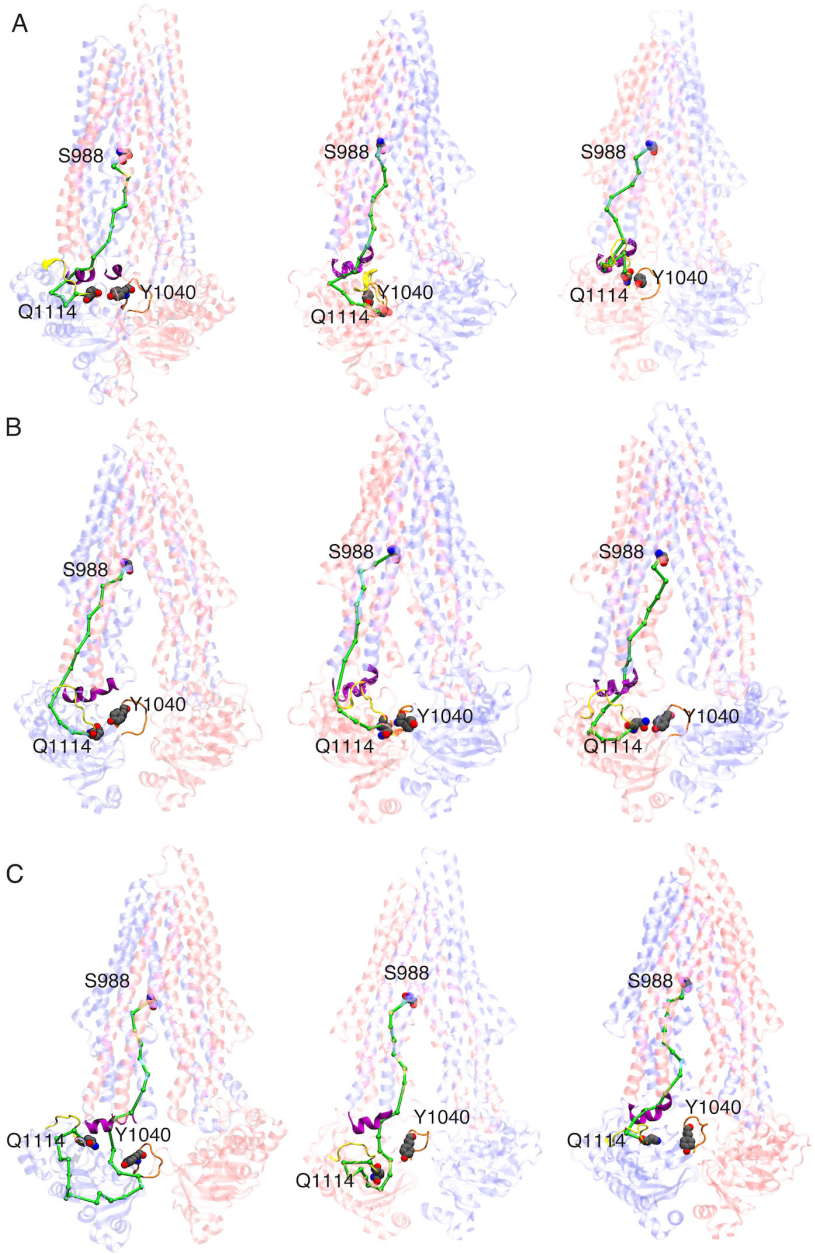

Figure 7: **Allosteric coupling between TMDs and NBDs:** The force propagation pathway calculated for all the three independent 500-ns simulations for: (A) ATP, (B) APO, and (C) TAR-bound Pgp systems, between the source S988 in TMD and sink Q1114 in NBD, is shown in green. Q-loop (containing conserved Q1114) is shown in yellow, coupling helices in purple, A-loop (containing conserved Y1040) in orange and the rest of the protein in a transparent cartoon representation. In the majority of TAR-bound simulations, extended pathways passing primarily through the coupling helices and the Q-loop in the NBDs are observed. Shorter and more direct pathways connecting the TMD and the NBD are observed in ATP and APO Pgp.

pathway connects the coupling helices with the A-loop, which contains a conserved aromatic residue (Y1040) critical for ATP binding.[58] As a result, the pathway transverses a larger portion of the NBD before reaching the Q-loop. In addition, by employing dynamic network analysis, communities, defining the set of residues that move in concert with each other during the simulations, were investigated. Similar communities were observed in the TMDs and the NBDs for all three systems (Fig. S8).

Discussion

Pgp actively extrudes xenobiotics across the plasma membrane. The transporter is overexpressed in a variety of cancer cells. It is closely associated with the development of drug resistance by interfering with the therapeutic targeting of the affected cells. As such, great effort is invested in developing novel strategies for targeting and inhibiting Pgp. In the present study, we have carried out an extensive set of all-atom MD simulations to characterize the conformational ensemble of Pgp in its native states (APO and ATP-bound) as well as in the presence of a third-generation inhibitor, TAR. We capture differential local and global conformational dynamics associated with the different bound states of Pgp, and, furthermore, we propose a novel lipid-dependent mechanism of action for the inhibitor.

The global orientational dynamics captured in our MD simulations of Pgp embedded in multi-component lipid bilayers, each starting from a different lipid distribution around Pgp, show dynamic equilibrium between open and closed NBD conformations of the transporter in the APO system, with the NBD twist angles showing large variations around the crystal structure values (Figs. 2 and S2). Along with dynamic NBDs, the transporter also samples distances corresponding to both open and closed TMDs in comparison to the crystal structure used to start the simulation, but remains relatively open with respect to the ATP-bound state. The APO systems also show higher lipid density inside the binding cavity of Pgp as well as a greater number of lipid-access events, which can be attributed to the more open

configuration of the TMD cytoplasmic gate (Fig. 4 and Fig. 5). As the substrates are believed to access the central binding cavity of Pgp largely from the lipid bilayer,[30] the APO state may allow recruitment of the substrates through the open cytoplasmic gate. In this context, the pathway observed in our simulations for the penetrating lipid molecules accessing the central cavity of Pgp may also represent a suitable route for the lateral translation and diffusion of the substrate molecules into the central cavity. The "wide-open" IF states of APO Pgp, frequently observed in experiments conducted using Pgp reconstitution in detergent or micellar environments,[27,31,59] confers it with no added physiological function and may portray artifacts of the non-physical (non-membrane) environments used in these experiments. The closed Pgp conformations captured in the APO simulations, on the other hand, have been recently characterized in cryoEM,[32] luminescence resonance energy transfer (LRET)[31] as well as atomic-force microscopy experiments (AFM),[30] with Pgp reconstituted in lipid nanodiscs or in liposomes, constituting a suitable membrane environment for the transporter.

In the ATP-bound systems, the conformational equilibrium is shifted towards closed-IF like states characterized by closure of the TMD cytoplasmic gate in addition to dimerization of the NBDs (Fig. 2 and Fig. S2). The ATP systems in our simulations lie close to the recent ATP-bound dimerized structure of human Pgp,[52] adopting a closed NBD conformation coupled to a closed TMD. Expectantly, a low lipid density is observed within the central cavity in the ATP systems which can be attributed to the closing of the cytoplasmic gate (Fig. 4 and Fig. 5). Substrate binding and subsequent binding of ATP to the NBDs in the APO systems may concurrently drive occlusion of the substrate-bound TMD and the closure of the inter-NBD gap,[34] in line with the conclusions of earlier mutagenesis and biochemical work.[31,60] Alternatively, ATP binding prior to the substrate entry may drive the transporter to a substrate-free occluded state, responsible for the known basal catalytic activity of the transporter.[61,62] A close interaction observed between the coupling helices in the TMDs and the Q-loop in the NBDs, observed in the ATP-bound systems compared to the APO

systems (Fig. 7), may allow fine-tuning of the concurrent movement in different domains of the transporter necessary for the transition to the OF state and completion of the transport cycle of Pgp, which is not fully observed here due to the limited timescale of the simulations.

From our systematic MD study, clear differences are observed in the conformational ensemble of Pgp in the presence of an inhibitor bound to the central cavity. In the presence of the inhibitor, Pgp becomes conformationally dynamic, both in the TMDs and the NBDs, sampling two major conformations, TAR_{wide} and TAR_{closed}, with different degrees of NBD dimerization (Fig. 2 and Fig. SS2). Two major Pgp conformations, characterized by distinct degrees of NBD opening, were also observed from the recent inhibitor-bound cryoEM structures,[34,55] with one of these structure showing NBD distances similar to TAR_{closed} conformations captured in our simulations.

Introduction of the inhibitor in the central cavity of Pgp, lying at the apex of the TMDs, also leads to an increase in the fluctuations of neighboring protein residues (Fig. S5), as well as local unfolding of the portal helix TM10 (Fig. 3), one of the helices present at the drug entry Portal 2 and involved in forming direct interactions with the inhibitor. The ZOS-bound cryo-EM structure shows a similar disorder in TM10 in the presence of the inhibitor,[34] although local unfolding in Portal 1 helices (TM4 and TM6) is also observed in this structure.

Compared to the transported substrates, Pgp inhibitors have been suggested to function by filling the drug-binding cavity more completely, while at the same time, forming a larger number of contacts with the binding residues.[34,63] Although the binding stoichiometry of TAR to Pgp is not well established, given its larger volume[9] and flexibility (more than twice rotatable bonds as compared to ZOS present in an inhibitor-bound cryoEM structure[34]), only one TAR molecule may suitably fit inside the central cavity of Pgp. The single TAR molecule may instead successfully fill the binding cavity through recruiting lipids, as seen from the increased lipid density and lipid access events inside the central cavity of Pgp in our TAR-bound simulations compared to APO and ATP-bound systems (Fig. 4, Fig. 5 and Supp. Video 1). Additionally, these "wedge-lipids", where the charged lipid head groups from the

cytoplasmic leaflet translocate inside the TMD while the lipid tails remain extended into the bulk membrane, are only observed in the inhibitor-bound systems (Fig. 6). The inhibitor may promote the recruitment of these wedge-lipids inside Pgp through a combination of conformational changes in the protein (larger TMD cytoplasmic gate and local unfolding of TM10, encouraging lipid diffusion and translation, and then directly forming interactions with the lipid head groups inside the central cavity.

A recent study using DEER spectroscopy showed that high-affinity, third generation inhibitors like TAR can differentially modulate the interactions between the A-loop and ATP compared to substrate-bound Pgp, in turn inhibiting ATP hydrolysis.[29] Previous cysteine-scanning mutagenesis study have shown that the long-range conformational changes in the NBDs can be regulated by inhibitors/substrates.[60] Additionally, lipid-binding sites observed at the regions formed by the kinking of the portal helices in response to inhibitor binding have been suggested to play a direct role in the modulation of Pgp function.[34] Inhibitor-mediated lipid diffusion resulting in wedge-lipids inside the central cavity of Pgp, as observed in our simulations, may contribute to the differential coupling observed in the inhibitor-bound simulations compared to the APO and ATP systems (Fig. 7), modulating the transfer of signal between the TMD and NBDs through the A-loop in case of the former. This may in turn play a disrupting role in the natural dynamics of the NBDs, preventing their correct interactions and dimerization and consequently inhibiting ATPase activity. In addition to directly restricting access to the substrate binding site, competitive inhibitors like TAR may thus successfully inhibit Pgp by stabilizing alternate occluded conformations of Pgp, halting or shifting the equilibrium away from reaching the OF states of the transporter.

Conclusion

As a multi-domain protein, Pgp displays a complex dynamical behavior, with the binding of ATP, substrates, inhibitors and surrounding lipidic environment modulating its confor-

mational ensemble. By employing extensive all-atom MD simulations, we show that that a third generation, high-affinity inhibitor, TAR, functions by allosterically modifying the conformational dynamics of the TMDs and NBDs, potentially inhibiting the transport cycle by disrupting the coupling between these two domains (Fig. 8). This additional mode of inhibition, which is complementary to the inhibitor's occupation of the substrate binding site, becomes amplified due to the inhibitor-mediated lipid diffusion and the recruitment of wedge lipids inside the central cavity of Pgp.

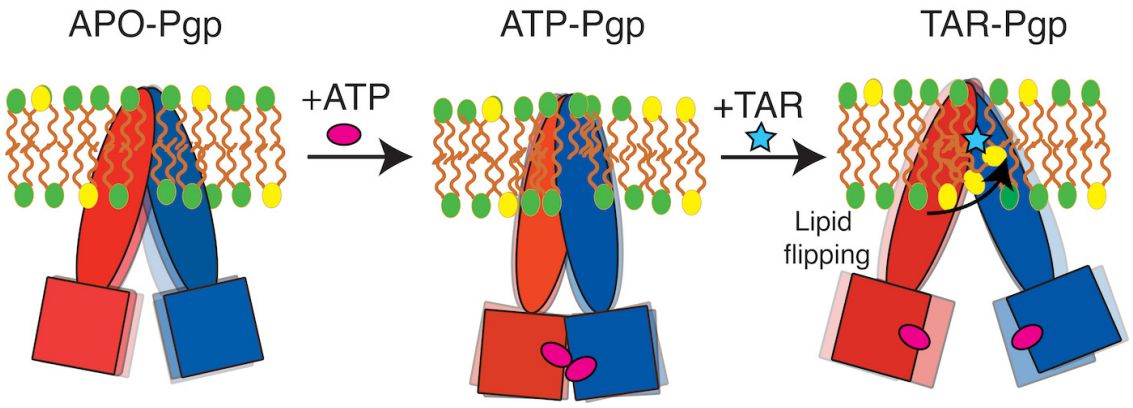

Figure 8: **Modulation of the conformational dynamics of Pgp by the lipidic environment and bound inhibitor**: In nucleotide-free (APO) state, Pgp exists in a dynamic equilibrium between open and closed IF conformations. ATP binding in the NBDs results in shifting of this dynamic equilibrium to predominantly closed IF conformations of Pgp. The presence of third-generation inhibitor (TAR) lead to lipid recruitment and flipping inside the central cavity of Pgp, thereby inhibiting NBD dimerization.

Furthermore, we show that the binding of ATP to the NBDs (in the absence of inhibitor) modifies the conformational dynamics of the transporter, favoring closed IF conformations, unlike APO Pgp, which exists in a dynamic equilibrium between open and closed IF conformations. The open IF conformations captured in the APO simulations, showing large cytoplasmic gate opening, may allow active recruitment of substrate molecules, whereas the closed IF conformations may allow formation of a suitable ATP binding pocket between the NBDs, promoting ATP binding and NBD dimerization.

Increase in multi-drug resistance in cancer cells calls for novel strategies for tackling this worldwide phenomenon. Understanding the secondary role of lipids in disrupting the function

of Pgp may provide novel points for the development of more potent and specific inhibitors that can further amplify lipid recruitment inside the binding cavity of the transporter. The results presented in the study will provide further motivation and direction to drug-discovery endeavours targeting challenging proteins like Pgp.

Acknowledgements

Research reported in this publication was supported by the National Institutes of Health under award numbers P41-GM104601 (to ET), and R01-GM123455 (to ET). We also acknowledge computing resources provided by Blue Waters at National Center for Supercomputing Applications, and Extreme Science and Engineering Discovery Environment (grant MCA06N060 to ET). S.P. would like to acknowledge Beckman Institute Graduate Fellowship for funding.

References

(1) Dean, M.; Hamon, Y.; Chimini, G. The human ATP-binding cassette (ABC) transporter superfamily. *Journal of Lipid Research* **2001**, *42*, 1007–1017.

(2) Vasiliou, V.; Vasiliou, K.; Nebert, D. W. Human ATP-binding cassette (ABC) transporter family. *Human genomics* **2009**, *3*, 281.

(3) Locher, K. P. Mechanistic diversity in ATP-binding cassette (ABC) transporters. *Nature Structural & Molecular Biology* **2016**, *23*, 487.

(4) Horio, M.; Gottesman, M. M.; Pastan, I. ATP-dependent transport of vinblastine in vesicles from human multidrug-resistant cells. *Proceedings of the National Academy of Sciences, USA* **1988**, *85*, 3580–3584.

(5) Busch, W.; Saier, M. H. The transporter classification (TC) system, 2002. *Critical reviews in biochemistry and molecular biology* **2002**, *37*, 287–337.

(6) Sharom, F. J. The P-glycoprotein multidrug transporter. *Essays in Biochemistry* **2011**, *50*, 161–178.

(7) Holland, I. B.; Blight, M. A. ABC-ATPases, adaptable energy generators fuelling transmembrane movement of a variety of molecules in organisms from bacteria to humans. *Journal of Molecular Biology* **1999**, *293*, 381–399.

(8) Sharom, F. J. Complex Interplay between the P-Glycoprotein Multidrug Efflux Pump and the Membrane: Its Role in Modulating Protein Function. *Frontiers in Oncology* **2014**, *4*, 1–19.

(9) Aller, S. G.; Yu, J.; Ward, A.; Weng, Y.; Chittaboina, S.; Zhuo, R.; Harrell, P. M.; Trinh, Y. T.; Zhang, Q.; Urbatsch, I. L.; Chang, G. Structure of P-Glycoprotein reveals a molecular basis for polyspecific drug binding. *Science* **2009**, *323*, 1718–1722.

(10) Jin, M. S.; Oldham, M. L.; Zhang, Q.; Chen, J. Crystal structure of the multidrug transporter P-glycoprotein from *Caenorhabditis elegans*. *Nature* **2012**, *490*, 566–569.

(11) Rosenberg, M. F.; Callaghan, R.; Modok, S.; Higgins, C. F.; Ford, R. C. Three-dimensional Structure of P-glycoprotein: the transmembrane regions adopt an asymmetric configuration in the nucleaotide-bound state. *Journal of Biological Chemistry* **2005**, *280*, 2857–2862.

(12) Li, J.; Jaimes, K. F.; Aller, S. G. Refined structures of mouse P-glycoprotein. *Protein Science* **2014**, *23*, 34–36.

(13) Mitchell, P. A general theory of membrane transport from studies of bacteria. *Nature* **1957**, *180*, 134–136.

(14) Jardetzky, O. Simple allosteric model for membrane pumps. *Nature* **1966**, *211*, 969–970.

(15) Dawson, R. J.; Locher, K. P. Structure of a bacterial multidrug ABC transporter. *Nature* **2006**, *443*, 180–185.

(16) Oldham, M. L.; Davidson, A. L.; Chen, J. Structural insights into ABC transporter mechanism. *Current Opinion in Structural Biology* **2008**, *18*, 726–733.

(17) Locher, K. P. Structure and mechanism of ATP-binding cassette transporters. *Philosophical Transactions of the Royal Society of London B. (Biological Sciences)* **2009**, *364*, 239–245.

(18) Hohl, M.; Briand, C.; Grütter, M. G.; Seeger, M. A. Crystal structure of a heterodimeric ABC transporter in its inward-facing conformation. *Nature Structural & Molecular Biology* **2012**, *19*, 395–402.

(19) Dawson, R. J.; Locher, K. P. Structure of the multidrug ABC transporter Sav1866 from *Staphylococcus aureus* in complex with AMP-PNP. *FEBS Letters* **2007**, *581*, 935–938.

(20) Ward, A.; Reyes, C. L.; Yu, J.; Roth, C. B.; Chang, G. Flexibility in the ABC transporter MsbA: alternating access with a twist. *Proceedings of the National Academy of Sciences, USA* **2007**, *104*, 19005–19010.

(21) Verhalen, B.; Dastvan, R.; Thangapandian, S.; Peskova, Y.; Koteiche, H. A.; Nakamoto, R. K.; Tajkhorshid, E.; Mchaourab, H. S. Energy Transduction and Alternating Access of the Mammalian ABC Transporter P-glycoprotein. *Nature* **2017**, *543*, 738–741.

(22) Jiang, T.; Wen, P.-C.; Trebesch, N.; Zhao, Z.; Pant, S.; Kapoor, K.; Shekhar, M.; Tajkhorshid, E. Computational Dissection of Membrane Transport at a Microscopic Level. *Trends in Biochemical Sciences* **2019**,

(23) Ambudkar, S. V.; Kimchi-Sarfaty, C.; Sauna, Z. E.; Gottesman, M. M. P-glycoprotein: from genomics to mechanism. *Oncogene* **2003**, *22*, 7468–7485.

(24) Sauna, Z. E.; Ambudkar, S. V. About a switch: how P-glycoprotein (ABCB1) harnesses the energy of ATP binding and hydrolysis to do mechanical work. *Molecular Cancer Therapeutics* **2007**, *6*, 13–23.

(25) Szöllősi, D.; Rose-Sperling, D.; Hellmich, U. A.; Stockner, T. Comparison of mechanistic transport cycle models of ABC exporters. *Biochimica et Biophysica Acta – Biomembranes* **2018**, *1860*, 818–832.

(26) Qu, Q.; Sharom, F. J. FRET Analysis Indicates That the Two ATPase Active Sites of the P-Glycoprotein Multidrug Transporter Are Closely Associated. *Biochemistry* **2001**, *40*, 1413–1422.

(27) Shukla, S.; Abel, B.; Chufan, E. E.; Ambudkar, S. V. Effects of a detergent micelle environment on P-glycoprotein (ABCB1)-ligand interactions. *Journal of Biological Chemistry* **2017**, *292*, 7066–7076.

(28) Li, M. J.; Guttman, M.; Atkins, W. M. Conformational dynamics of P-glycoprotein in lipid nanodiscs and detergent micelles reveal complex motions on a wide time scale. *Journal of Biological Chemistry* **2018**, *293*, 6297–6307.

(29) Dastvan, R.; Mishra, S.; Peskova, Y. B.; Nakamoto, R. K.; Mchaourab, H. S. Mechanism of allosteric modulation of P-glycoprotein by transport substrates and inhibitors. *Science* **2019**, *364*, 689–692.

(30) Sigdel, K.; Wilt, L.; Marsh, B.; Roberts, A.; King, G. The conformation and dynamics of P-glycoprotein in a lipid bilayer investigated by atomic force microscopy. *Biochemical Pharmacology* **2018**, *156*, 302–311.

(31) Zoghbi, M. E.; Mok, L.; Swartz, D. J.; Singh, A.; Fendley, G. A.; Urbatsch, I. L.; Altenberg, G. A. Substrate-induced conformational changes in the nucleotide-binding domains of lipid bilayer–associated P-glycoprotein during ATP hydrolysis. *Journal of Biological Chemistry* **2017**, *292*, 20412–20424.

(32) Frank, G. A.; Shukla, S.; Rao, P.; Borgnia, M. J.; Bartesaghi, A.; Merk, A.; Mobin, A.; Esser, L.; Earl, L. A.; Gottesman, M. M., et al. Cryo-EM analysis of the conformational landscape of human P-glycoprotein (ABCB1) during its catalytic cycle. *Molecular Pharmacology* **2016**, *90*, 35–41.

(33) Palmeira, A.; Vasconcelos, M. H.; Paiva, A.; Fernandes, M. X.; Pinto, M.; Sousa, E. Dual inhibitors of P-glycoprotein and tumor cell growth: (Re)discovering thioxanthones. *Biochemical Pharmacology* **2012**, *83*, 57–68.

(34) Alam, A.; Kowal, J.; Broude, E.; Roninson, I.; Locher, K. P. Structural insight into substrate and inhibitor discrimination by human P-glycoprotein. *Science* **2019**, *363*, 753–756.

(35) Wen, P.-C.; Verhalen, B.; Wilkens, S.; Mchaourab, H. S.; Tajkhorshid, E. On the origin of large flexibility of P-glycoprotein in the inward-facing state. *Journal of Biological Chemistry* **2013**, *288*, 19211–19220.

(36) Zaitseva, J.; Jenewein, S.; Jumpertz, T.; Holland, I. B.; Schmitt, L. H662 is the linchpin of ATP hydrolysis in the nucleotide-binding domain of the ABC transporter HlyB. *EMBO Journal* **2005**, *24*, 1901–1910.

(37) Moradi, M.; Tajkhorshid, E. Computational recipe for efficient description of large-scale conformational changes in biomolecular systems. *Journal of Chemical Theory and Computation* **2014**, *10*, 2866–2880.

(38) Jo, S.; Kim, T.; Iyer, V. G.; Im, W. CHARMM-GUI: a web-based graphical user interface for CHARMM. *Journal of Computational Chemistry* **2008**, *29*, 1859–1865.

(39) Phillips, J. C.; Braun, R.; Wang, W.; Gumbart, J.; Tajkhorshid, E.; Villa, E.; Chipot, C.; Skeel, R. D.; Kale, L.; Schulten, K. Scalable molecular dynamics with NAMD. *Journal of Computational Chemistry* **2005**, *26*, 1781–1802.

(40) Phillips, J. C.; Hardy, D. J.; Maia, J. D. C.; Stone, J. E.; Ribeiro, J. V.; Bernardi, R. C.; Buch, R.; Fiorin, G.; Hénin, J.; Jiang, W.; McGreevy, R.; Melo, M. C. R.; Radak, B.; Skeel, R. D.; Singharoy, A. et al. Scalable molecular dynamics on CPU and GPU architectures with NAMD. *Journal of Chemical Physics* **2020**, *153*, 044130.

(41) Best, R. B.; Zhu, X.; Shim, J.; Lopes, P. E. M.; Mittal, J.; Feig, M.; MacKerell, A. D. Optimization of the additive CHARMM all-atom protein force field targeting improved sampling of the backbone ϕ, ψ and side-chain χ_1 and χ_2 dihedral angles. *Journal of Chemical Theory and Computation* **2012**, *8*, 3257–3273.

(42) Klauda, J. B.; Venable, R. M.; Freites, J. A.; O'Connor, J. W.; Tobias, D. J.; Mondragon-Ramirez, C.; Vorobyov, I.; MacKerell Jr., A. D.; Pastor, R. W. Update of the CHARMM all-atom additive force field for lipids: validation on six lipid types. *Journal of Physical Chemistry B* **2010**, *114*, 7830–7843.

(43) Jorgensen, W. L.; Chandrasekhar, J.; Madura, J. D.; Impey, R. W.; Klein, M. L. Comparison of Simple Potential Functions for Simulating Liquid Water. *Journal of Chemical Physics* **1983**, *79*, 926–935.

(44) Mayne, C. G.; Saam, J.; Schulten, K.; Tajkhorshid, E.; Gumbart, J. C. Rapid parameterization of small molecules using the Force Field Toolkit. *Journal of Computational Chemistry* **2013**, *34*, 2757–2770.

(45) Humphrey, W.; Dalke, A.; Schulten, K. VMD – Visual Molecular Dynamics. *Journal of Molecular Graphics* **1996**, *14*, 33–38.

(46) Møller, C.; Plesset, M. S. Note on an Approximation Treatment for Many-Electron Systems. *Physical Review* **1934**, *46*, 618–622.

(47) Frisch, M. J.; Trucks, G. W.; Schlegel, H. B.; Scuseria, G. E.; Robb, M. A.; Cheeseman, J. R.; Scalmani, G.; Barone, V.; Mennucci, B.; Petersson, G. A.; Nakatsuji, H.; Caricato, M.; Li, X.; Hratchian, H. P.; Izmaylov, A. F. et al. *Gaussian 09, Revision B.01*; Gaussian, Inc., Wallingford CT, 2010.

(48) Dolinsky, T. J.; Nielsen, J. E.; McCammon, J. A.; Baker, N. A. PDB2PQR: an automated pipeline for the setup of Poisson-Boltzmann electrostatics calculations. *Nucleic Acids Research* **2004**, *32*, W665–W667.

(49) Martyna, G. J.; Tobias, D. J.; Klein, M. L. Constant pressure molecular dynamics algorithms. *Journal of Chemical Physics* **1994**, *101*, 4177–4189.

(50) Essmann, U.; Perera, L.; Berkowitz, M. L.; Darden, T.; Lee, H.; Pedersen, L. G. A smooth particle mesh Ewald method. *Journal of Chemical Physics* **1995**, *103*, 8577–8593.

(51) Moradi, M.; Tajkhorshid, E. Mechanistic picture for conformational transition of a membrane transporter at atomic resolution. *Proceedings of the National Academy of Sciences, USA* **2013**, *110*, 18916–18921.

(52) Kim, Y.; Chen, J. Molecular structure of human P-glycoprotein in the ATP-bound, outward-facing conformation. *Science* **2018**, *359*, 915–919.

(53) Sethi, A.; Eargle, J.; Black, A. A.; Luthey-Schulten, Z. Dynamical networks in tRNA:protein complexes. *Proceedings of the National Academy of Sciences, USA* **2009**, *106*, 6620–6625.

(54) Davidson, A. L.; Dassa, E.; Orelle, C.; Chen, J. Structure, Function, and Evolution of Bacterial ATP-Binding Cassette Systems. *Microbiology and Molecular Biology Reviews* **2008**, *72*, 317–364.

(55) Alam, A.; Kung, R.; Kowal, J.; McLeod, R. A.; Tremp, N.; Broude, E. V.; Roninson, I. B.; Stahlberg, H.; Locher, K. P. Structure of a zosuquidar and UIC2-bound human-mouse chimeric ABCB1. *Proc Natl Acad Sci USA* **2018**, *115*, 1973–1982.

(56) Barreto-Ojeda, E.; Corradi, V.; Gu, R.-X.; Tieleman, D. P. Coarse-grained molecular dynamics simulations reveal lipid access pathways in P-glycoprotein. *Journal of General Physiology* **2018**, *150*, 417–429.

(57) Wilkens, S. Structure and mechanism of ABC transporters. *F1000Research* **2015**, *7*.

(58) Ambudkar, S. V.; Kim, I.-W.; Xia, D.; Sauna, Z. E. The A-loop, a novel conserved aromatic acid subdomain upstream of the Walker A motif in ABC transporters, is critical for ATP binding. *FEBS Letters* **2006**, *580*, 1049–1055.

(59) Li, S.; Jang, H.; Zhang, J.; Nussinov, R. Raf-1 Cysteine-Rich Domain Increases the Affinity of K-Ras/Raf at the Membrane, Promoting MAPK Signaling. *Structure* **2018**, *26*, 513 – 525.e2.

(60) Loo, T. W.; Bartlett, M. C.; Clarke, D. M. Simultaneous Binding of Two Different Drugs in the Binding Pocket of the Human Multidrug Resistance P-glycoprotein. *Journal of Biological Chemistry* **2003**, *278*, 39706–39710.

(61) Al-Shawi, M. K.; Polar, M. K.; Omote, H.; Figler, R. A. Transition state analysis of the coupling of drug transport to ATP hydrolysis by P-glycoprotein. *Journal of Biological Chemistry* **2003**, *278*, 52629–52640.

(62) Esser, L.; Zhou, F.; Pluchino, K. M.; Shiloach, J.; Ma, J.; Tang, W.-k.; Gutierrez, C.; Zhang, A.; Shukla, S.; Madigan, J. P.; Zhou, T.; Kwong, P. D.; Ambudkar, S. V.; Gottesman, M. M.; Xia, D. Structures of the multidrug transporter P-glycoprotein reveal asymmetric ATP binding and the mechanism of polyspecificity. *Journal of Biological Chemistry* **2017**, *292*, 446–461.

(63) Loo, T. W.; Clarke, D. M. Mapping the binding site of the inhibitor tariquidar that stabilizes the first transmembrane domain of P-glycoprotein. *Journal of Biological Chemistry* **2015**, *290*, 29389–29401.

Supporting Information

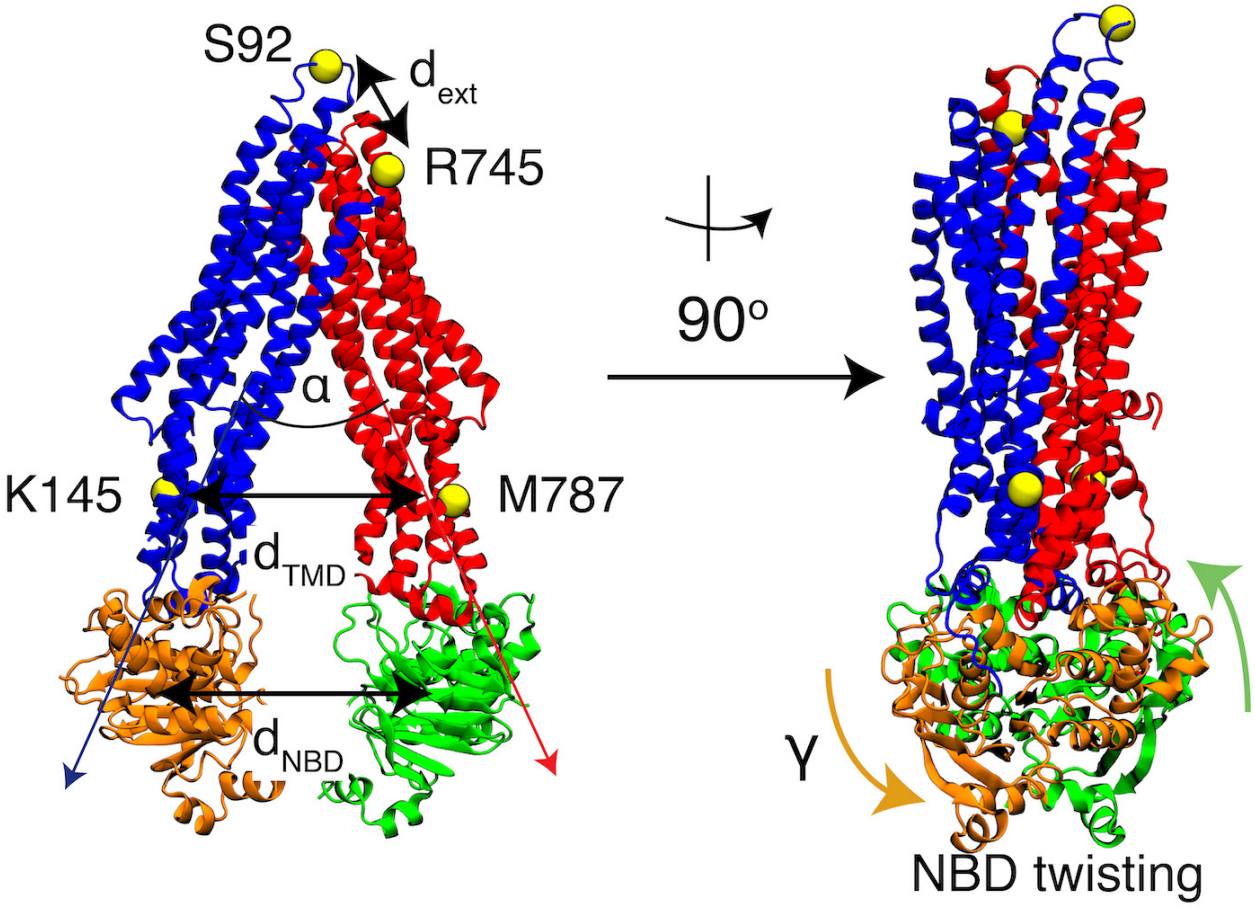

Figure S1: **Definitions of the reaction coordinates used to characterize global dynamics of Pgp.** Cartoon representation of Pgp in an IF conformation along with the definitions of reaction coordinates used for monitoring the global conformational dynamics in the protein: d_{TMD} (center of mass distance between Cα atoms of K145 and M787 on the cytoplasmic side of the TMDs), d_{ext} (center of mass distance between Cα atoms of S92 and R745 on the extracellular end), d_{NBD} (center of mass distance of the two NBDs), α (angle describing cytoplasmic closing of the TMDs), and γ (NBD twisting). NBDs are colored in orange/green and TMDs are colored in red/blue.

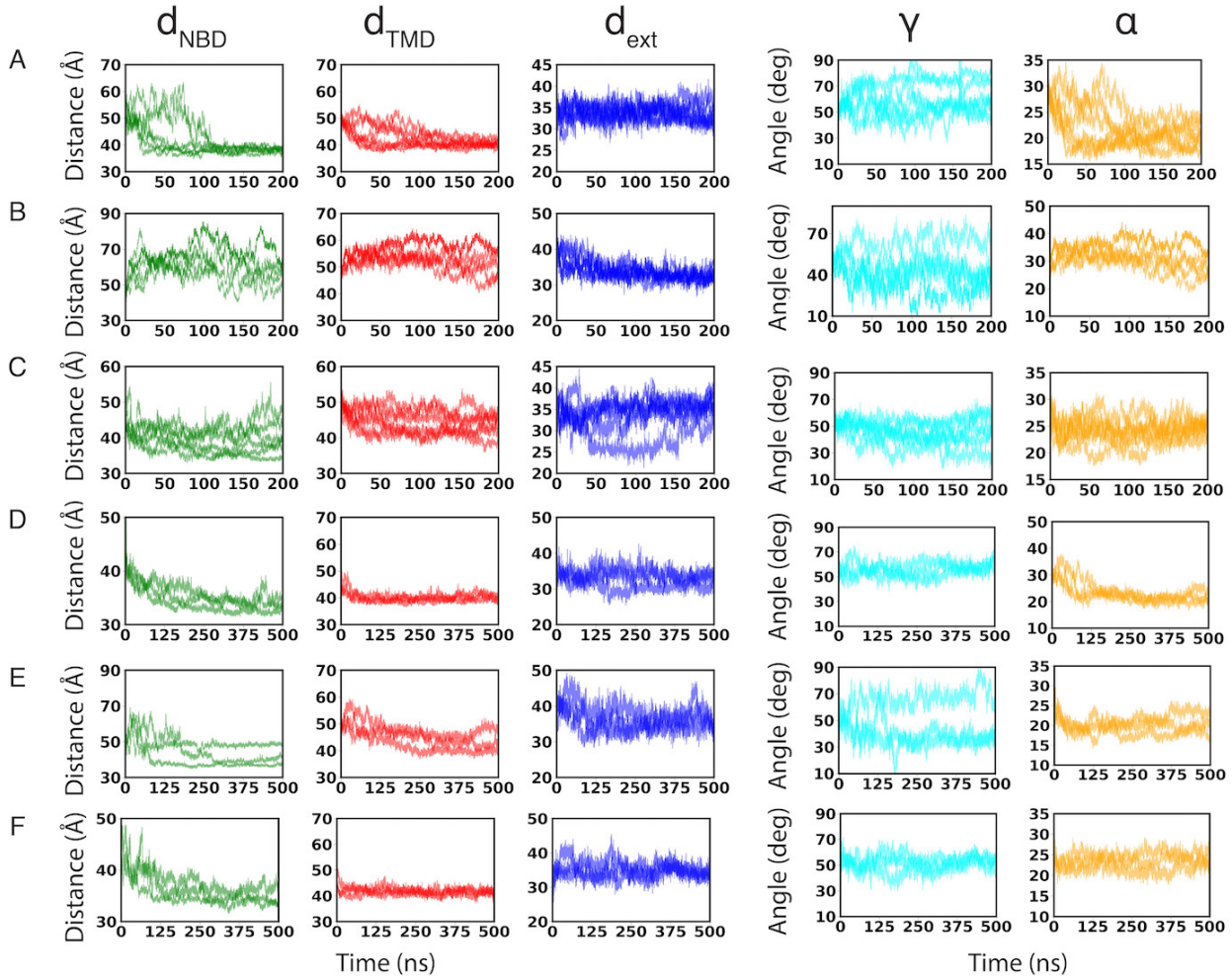

Figure S2: **Global conformational dynamics in Pgp:** Time evolution of the geometric parameters (see Fig. S1 for definitions) used to characterize the global conformational dynamics of Pgp for 200-ns long simulations in (A) ATP, (B) TAR-bound, (C) APO Pgp, and for 500-ns simulations in (D) ATP, (E) TAR-bound, (F) APO Pgp. The global conformational changes are defined by d_{NBD} (green), d_{TMD} (red), d_{ext} (blue), γ (cyan), and α (orange).

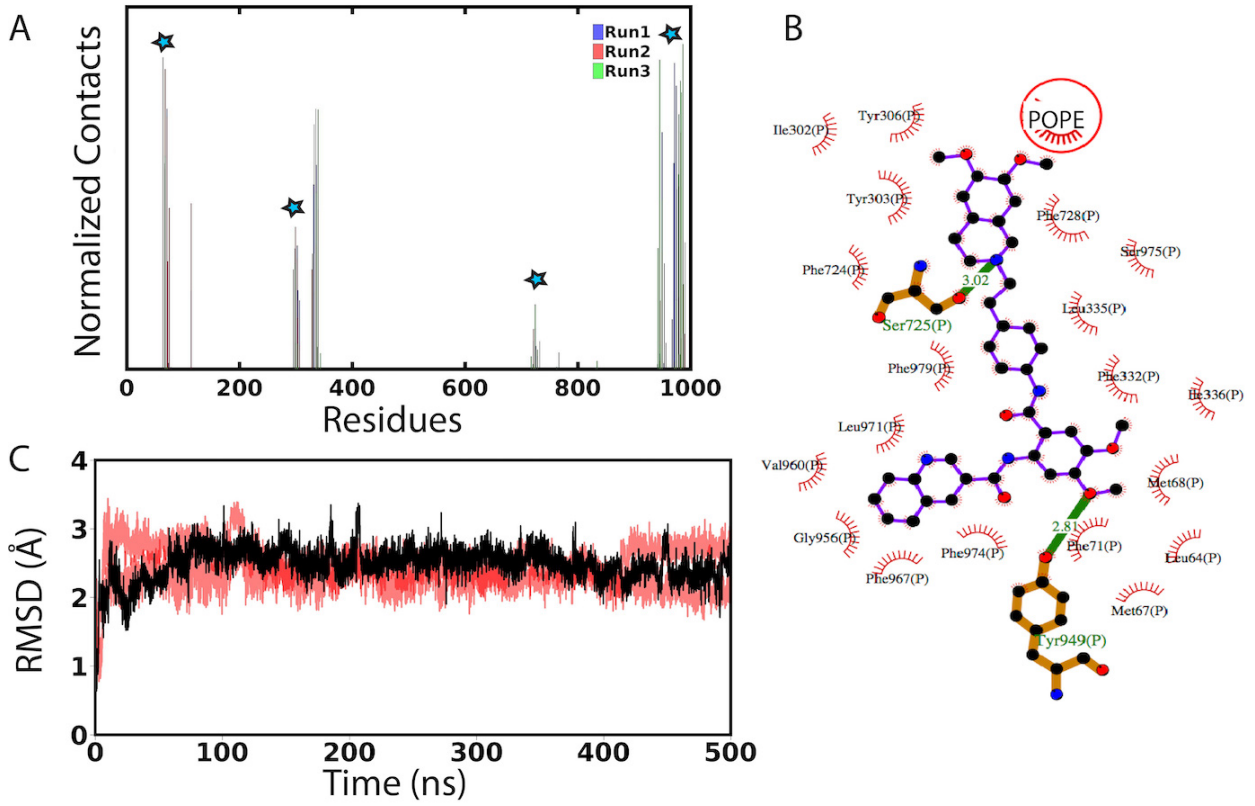

Figure S3: **TAR–Pgp interactions:** (A) All Pgp residues interacting with the inhibitor in 500-ns simulations are shown. For comparison, the region of Pgp also found to be interacting with another third-generation inhibitor, zosuquidar, from a recent cryoEM structure (PDB:6FN1),[55] are shown with cyan stars. (B) Interaction of TAR with the surrounding residues of Pgp as captured in one of the simulations. The TAR-binding pocket is predominantly rich in hydrophobic residues. Two polar side chains, Y949 and S725, form hydrogen bonds with the bound inhibitor. The position of a wedge-lipid POPE is shown in red circle. (C) The stability of the bound TAR molecule was calculated by measuring the heavy atom RMSD of TAR in all the simulations. One representative trajectory is shown in black and other trajectories are shown in red. In all simulations, a stable mode of binding for the inhibitor was observed in the central cavity of Pgp.

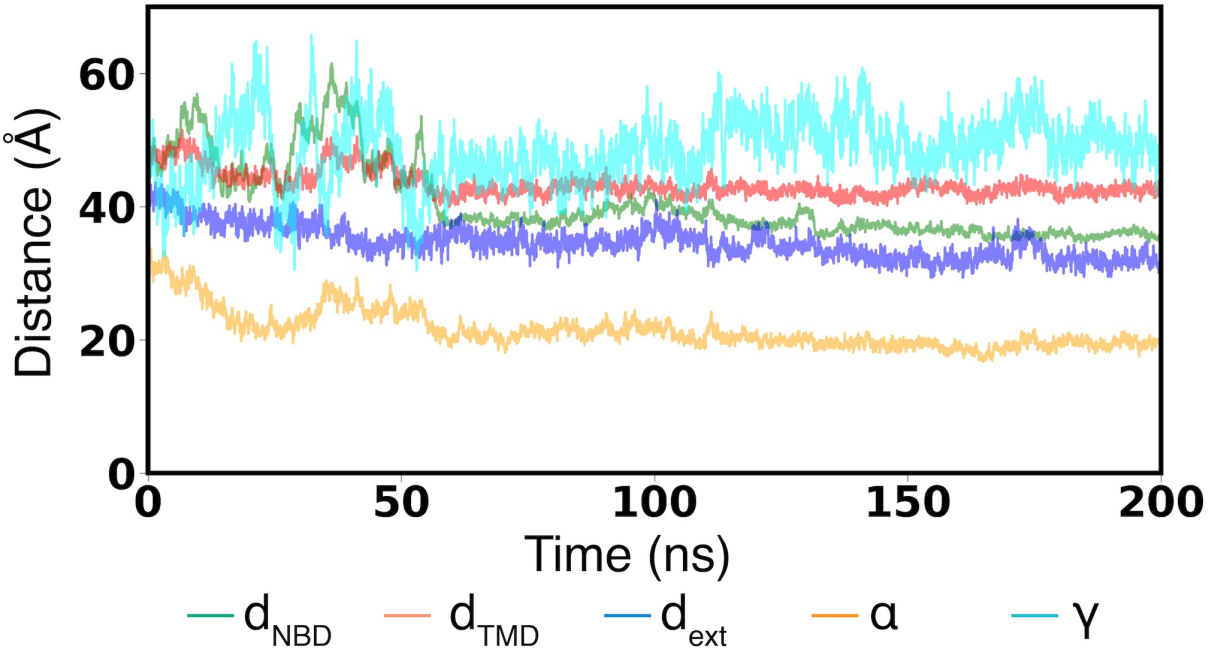

Figure S4: **Conformational dynamics of Pgp in control simulation:** Time evolution of the global conformational changes in TAR-bound Pgp conformation after removing the bound inhibitor. These changes are defined by d_{NBD} (green), d_{TMD} (red), d_{ext} (blue), γ (cyan), and α (orange). After removing TAR, the structure shows conformational dynamics similar to ATP-bound Pgp, with no lipid flipping events observed inside the central cavity.

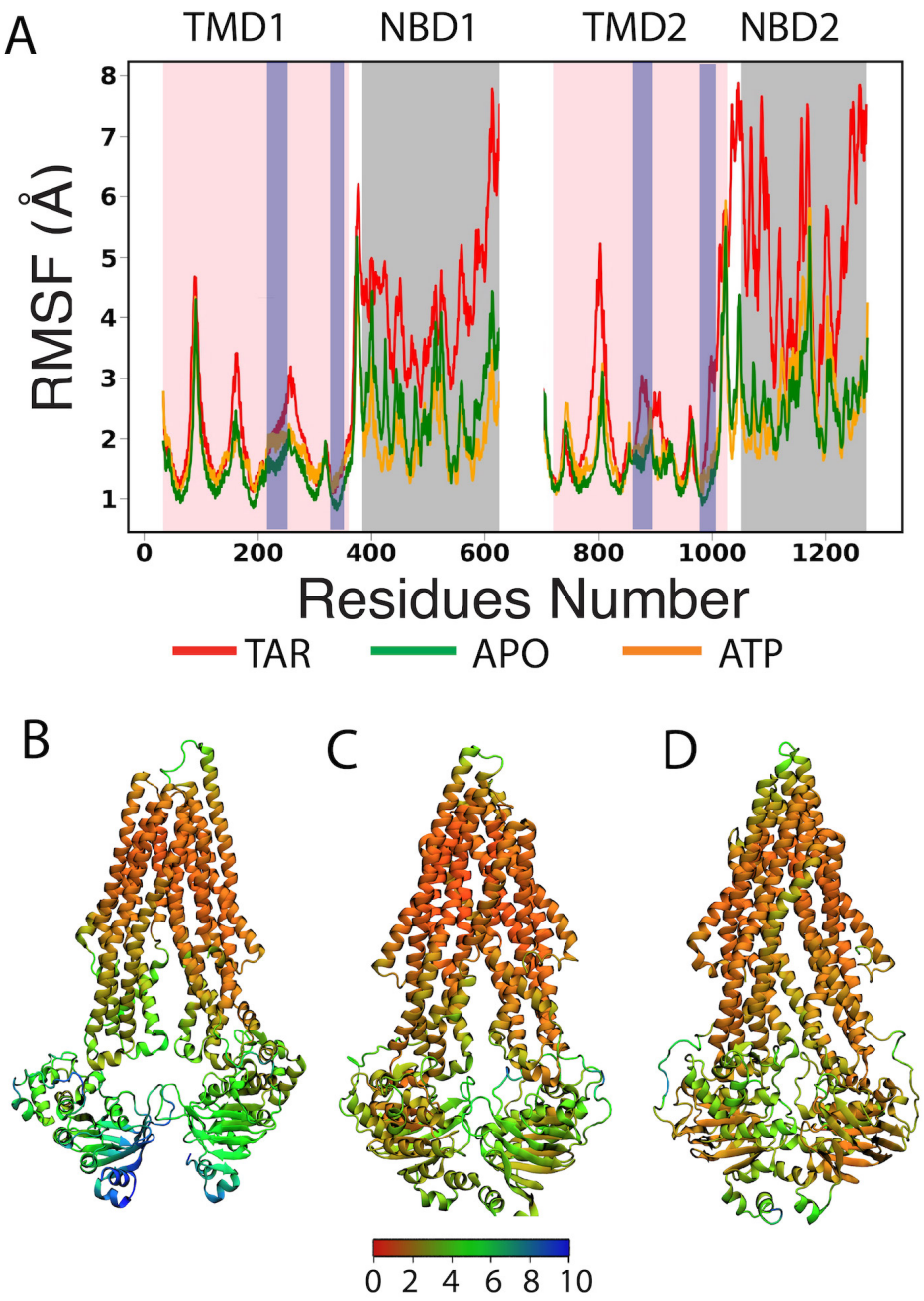

Figure S5: **Pgp fluctuations captured from MD simulations:** (A) RMSF calculated for the three bound states combining all the three 500-ns MD trajectories for each state. The heatmap of the RMSF analysis shown for (B) TAR-bound, (C) ATP, and (D) APO Pgp. Color bar for the change is shown at the bottom. Compared to ATP-bound and APO Pgp, overall higher RMSF values are observed in TAR-bound systems, especially in the TMD portal helices and NBDs (highlighted in blue and grey backgrounds in (A), respectively).

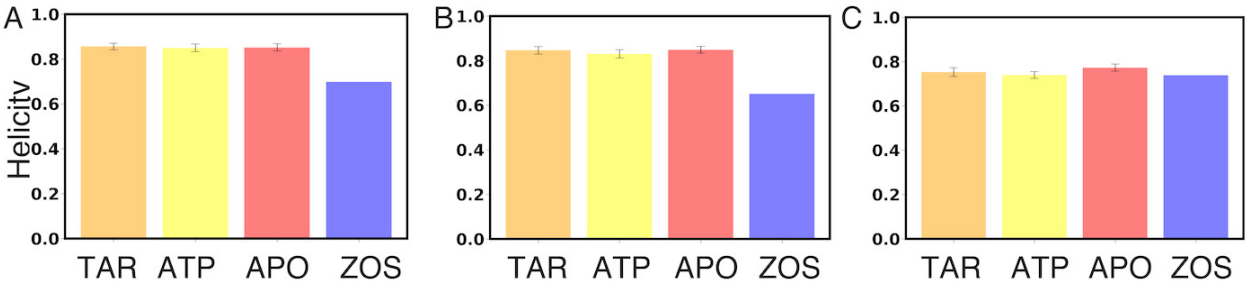

Figure S6: **Local changes in secondary structure:** Comparison of the degrees of helicity in TM4 (A), TM6 (B), and TM12 (C) in APO, ATP, and TAR-bound Pgp with the zosuquidar-bound cryoEM structure.[55] For all three portal helices, similar degrees of helicity was observed in all three simulated systems. As compared to zosuquidar-bound Pgp, no loss in the helicity in TM4 and TM6 was observed.

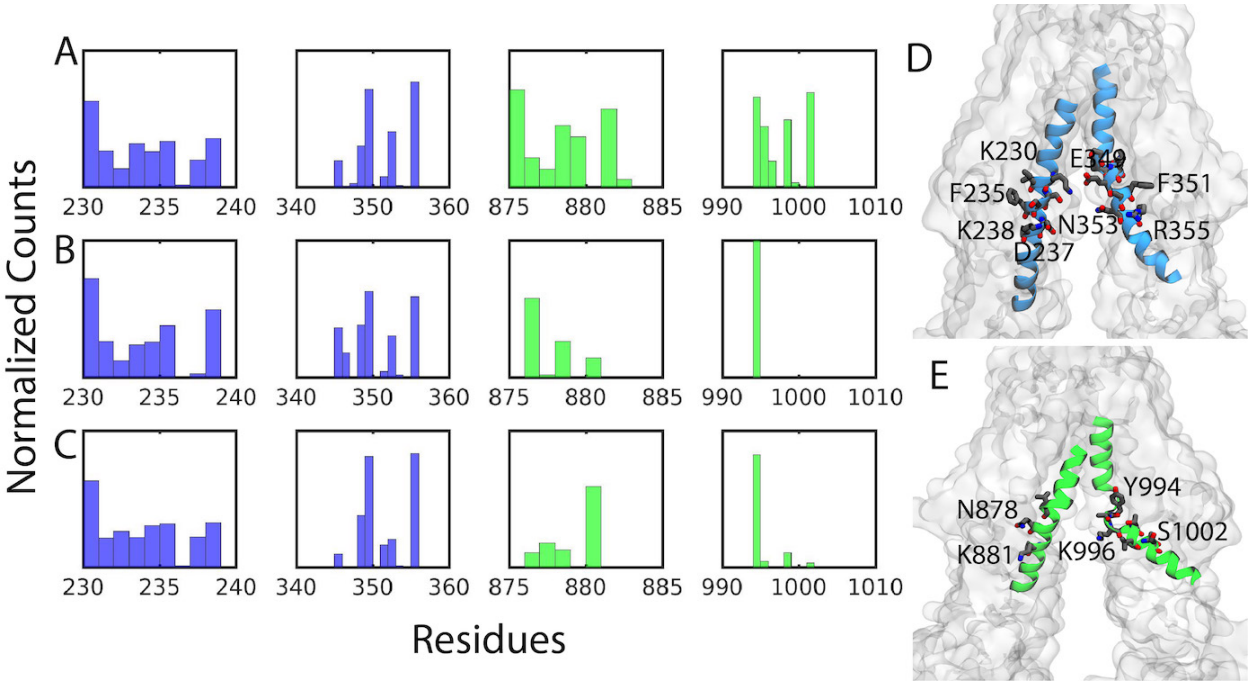

Figure S7: **Lipid-interacting residues at the entry portals:** Residues in Portals 1 and 2, shown in blue and green, respectively, making contacts with penetrating lipids over the course of one 500-ns simulation in TAR-bound (A), ATP (B), and APO Pgp (C). All the portal residues making contact for more than 20% of the simulation time are shown in (D) for Portal 1, and in (E) for Portal 2. Most of the lipid-interacting sites are rich in basic residues. As compared to Portal 1, less contacts were observed in Portal 2.

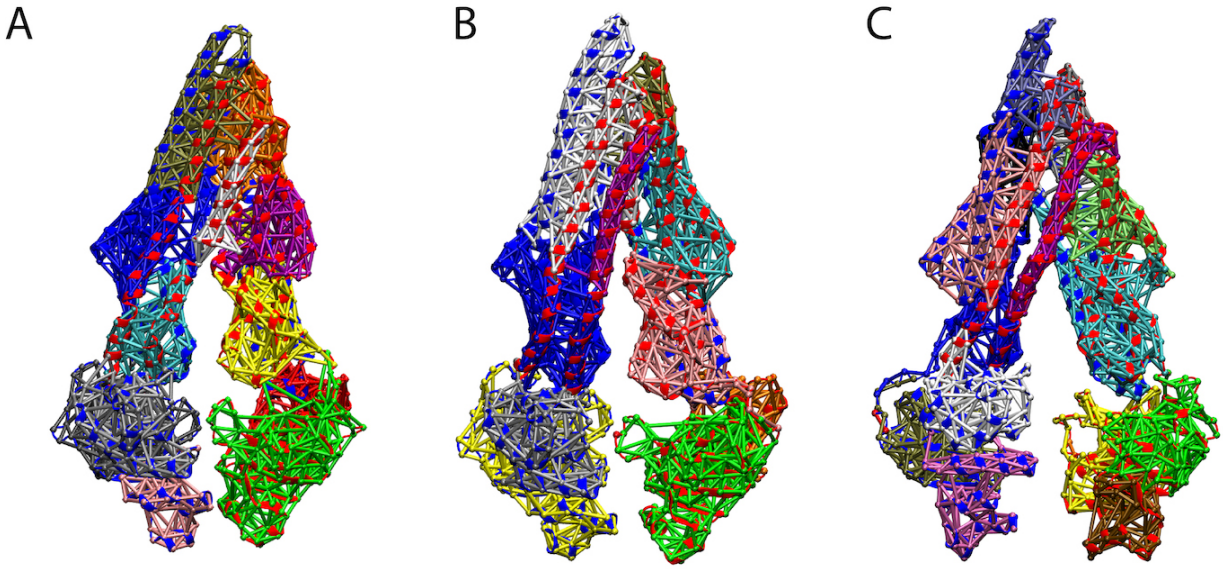

Figure S8: **Network-based community analysis:** Community analysis in the APO (A), ATP-bound (B), and TAR-bound (C) Pgp showing regions with high internal correlation during the 500-ns MD simulation. The communities are individually colored and show similar behavior in all three systems.